Retrieval of Land Surface Parameters Using Passive Microwave Measurements at 6 to 18 GHz

Eni G. Njoku and Li Li

Jet Propulsion Laboratory, M/S 300-233
4800 Oak Grove Drive, Pasadena, CA 91109
Phone: (818) 453-3693
Fax: (818) 354-9476
E-mail: eni.g.njoku@jpl.nasa.gov

Submitted for publication to:
IEEE Transactions on Geoscience and Remote Sensing

July 12, 1997

Jet Propulsion Laboratory
California Institute of Technology
Pasadena, CA

ABSTRACT

An approach is evaluated for retrieval of land surface parameters (soil moisture, vegetation water content, and surface temperature) using satellite microwave radiometer data in the 6 to 18 GHz frequency range. The approach is applicable to data that will be acquired by the Advanced Microwave Scanning Radiometer (AMSR), planned for launch on the ADEOS-II and EOS PM-1 satellites in 1999 and 2000, respectively. The retrieval method is based on a radiative transfer model for land-surface and atmospheric emission, with model coefficients that can be tuned over specific calibration regions and applied globally. The method uses an iterative, least squares algorithm, based on six channels of radiometric data. Simulations using this algorithm indicate that, for an assumed sensor noise of 0.3 K in all channels, soil moisture and vegetation water content retrieval accuracies of 0.06 g cm^{-3} and 0.15 kg m^{-2}, respectively, should be achievable in regions of vegetation water content less than approximately 1.5 kg m^{-2}. A surface temperature accuracy of 2 C should be achievable, except for bare soils where discrimination between moisture and temperature variability is difficult using this algorithm. These accuracies are for retrievals averaged over the sensor footprint, and exclude conditions of precipitation, open water, snow cover, frozen ground, or high topographic relief within the footprint. The algorithm has been tested using data from the Nimbus-7 Scanning Multichannel Microwave Radiometer (SMMR) for the years 1982-85, over the African Sahel, and the retrieval results compared to output from an operational numerical weather prediction model. The retrieval algorithm is shown to discriminate well between soil moisture, vegetation, and temperature variations, and to provide estimates consistent with the expected accuracies. Future work will investigate possible improvements to the algorithm using alternate formulations, possibly with fewer channels, and will extend testing of the algorithm to other regions.

I. INTRODUC ['[ON

As part of its Mission To Planet Earth (MTPE), NASA plans to launch the Advanced Microwave Scanning Radiometer (AMSR) on the Earth Observing System (EOS) PM-1 satellite in late 2000. The EOS AMSR (AMSR-E) is a modified version of the AMSR instrument designed for launch on the Japanese Advanced Earth Observing Satellite-II (ADEOS-II) in 1999. The two AMSR instruments will operate in polar, sun-synchronous orbits, with equator crossings at 10:30 am and 1:30 pm for AMSR and AMSR-E respectively. The AMSR is a successor in technology to the Scanning Multichannel Microwave Radiometer (SMMR) and Special Sensor Microwave Imager (SSM/I) instruments, first launched in 1978 and 1987 respectively, and will provide observations of variables describing the Earth's atmosphere, ocean, cryosphere, and land surface. Over snow-free land, it will be possible to estimate three surface variables from AMSR data: surface soil moisture, m_e; vegetation water content, w_e; and surface temperature, T_e. Observations by AMSR of these variables will be of benefit to applications involving surface energy and water balance, large-scale hydrologic modeling, numerical weather prediction, climate modeling, and monitoring of floods, droughts, and land-cover change. In this paper we describe an approach for estimating m_e, w_e, and T_e from the 6 to 18 GHz AMSR channels, and test the method using historical SMMR data.

Recent studies have shown the effects of soil moisture on the dynamics of the atmospheric boundary layer and hence on weather and climate. Such studies have also shown the influence of soil moisture on the feedbacks between land-surface and atmospheric processes that lead to climate anomalies [1]-[3]. Simulations have shown that improved characterizations of surface soil moisture, vegetation, and temperature in numerical weather-prediction models lead to significant forecast improvements [e.g. 4]. For these reasons, the lack of a global hydrologic land-surface observing capability has been recognized as a limitation on improved climate forecasting

and monitoring. Soil moisture has become a key measurement priority of NASA's MTPE program [5]. AMSR measurements will contribute to such an observing capability.

The current generation of spaceborne radiometers are not optimal for land sensing in terms of spatial resolution and frequency, especially for soil moisture sensing. The SMMR, launched on the Nimbus-7 satellite in 1978, had a spatial resolution of -150 km at its lowest frequency of 6.6 GHz [6]. The SSM/I, launched in 1987, has a lowest frequency of 19.3 GHz [7], at which vegetation cover can dominate the soil moisture signal. Low frequencies (below -3 GHz) are preferable for soil moisture sensing, since the attenuation through vegetation is less and the sensitivity to moisture below the top centimeter of soil is greater, at lower frequencies [8]. Under low-vegetation conditions, however, the 6.6 and 10.7 GHz channels of the SMMR (similar to the two low-frequency AMSR channels) have adequate sensitivity to surface soil moisture. In this paper we emphasize the use of the two low frequencies for soil moisture sensing. We also include the 18 GHz frequency for its anticipated additional sensitivity to low vegetation amounts and to surface temperature. The spatial resolution provided by AMSR (-70 km at 6.9 GHz) is an improvement over the SMMR, and is reasonably matched to the grid scales of the current global atmospheric general circulation models (-50 to 100 km). "l'he comparative operating characteristics of the SMMR, SSM/I, and AMSR are shown in Table 1.

AMSR measurements of surface temperature and vegetation will complement similar measurements of these parameters obtained from optical and thermal-infrared sensors on the EOS PM- 1 platform (i.e. MODI S and AIRS). Although passive-microwave measurements are of lower spatial resolution than optical and infrared measurements, they are less influenced by solar illumination, aerosols, and clouds, and are responsive to different dynamic ranges of vegetation structure and biomass. Thus, there is potential for synergistic usc of products derived from the AMSR, MODIS, and AIRS instruments.

Algorithms developed to retrieve land parameters from AMSR at 6 to 18 GHz can be tested using the historical SM MR data record since the S MM R operated at similar frequencies to

AMSR. SSM/I data cannot be used for this purpose since the SSM/I does not have channels near 6 and 10 GHz. In this paper wc focus on estimating m_e, w_e, and T_e using the 6 to 18 GHz channels, and test the procedure using SM MR data (available from 1979 to 1987) over the African Sahel.

The procedure for deriving m_e, w_e, and T_e is based on a physical model of microwave emission from a layered soil-vegetation-atmosphere medium. The model exhibits a nonlinear dependence on vegetation, hence an iterative least-squares-minimization retrieval method is employed. For satellite applications, the retrieved variables are area-averages over the footprint. Strictly speaking, the retrievals of m_e and T_e also represent vertically-weighted averages over the sampling depths in the soil and vegetation. Certain parameters of the physical model, such as soil surface roughness and vegetation single-scattering albedo, cannot be measured easily, and hence must be estimated from physical principles or derived empirically, a-priori. These parameters can be assigned uncertainty estimates, enabling an overall estimate to be made of the geophysical retrieval accuracies. As the vegetation cover increases, the retrieval errors for m_e and w_e increase also, and for dense vegetation these variables cannot be retrieved reliably. The retrieval algorithm identifies when the reliability thresholds have been exceeded.

Terminologies and parameterizations used in describing the surface soil and vegetation states are often not well defined or consistently applied in radiative transfer and hydrometeorological modeling. The term “soil wetness” is often used to describe the amount of soil water computed from a meteorological land-surface model. I Iowever, the soil wetness so defined is model-dependent, since different models can give different values of soil wetness while having similar estimates of water and energy exchange. Also, the soil depth within which the soil wetness is defined varies according to the model [9]. When referring to land-surface temperature, the terms “canopy temperature”, “skin temperature”, “aerodynamic temperature”, and “radiation temperature” may be implied, according to the context, The interpretation may depend on the model being used, the viewing direction and wavelength of the sensor, and the 3-dimensional

characteristics of the surface [10]. Similarly, various parameters have been used to describe vegetation state, including "biomass", "leaf-area index" (LAI), "normalized difference vegetation index" (NDVI), etc. In this paper, the microwave-derived variables m_e, T_e, and w_e, are defined, but no attempt is made here to relate these explicitly to the parameters of other sensors and models. For synergistic studies this will have to be done, however.

II. Historical Perspective

The potential of the 6.6 and 10.7 GHz channels of the SMMR for soil moisture monitoring was first investigated by Wang [11] and Njoku and Patel [12]. These studies were followed by others [13]-[17]. S M M R data were also shown to be useful for monitoring seasonal flooding [18], and for vegetation monitoring [19], [20]. McFarland et al. [21] and others [20], [22] showed that SMMR and SSM/I data could be used to estimate surface temperature. The effects of the intervening atmosphere on land-surface measurements at 37 GH z were also investigated [23], [24]. Ferraro et al. [25], Neale et al. [26], and others, have investigated surface type classifications obtainable using SMMR and SSM/I data. The effects of surface heterogeneity on passive land retrievals have been studied by Njoku et al. [27]. In this paper we build on these investigations by providing a method for quantitative retrieval of moisture, temperature, and vegetation parameters over snow-free land, using an algorithm that can eventually be applied globally for climate modeling and monitoring applications. Recent studies have also considered approaches for assimilating satellite microwave radiances directly into predictive models of moisture and heat flow in soils and ecosystem functioning [28], [29]. In this manner, microwave radiative transfer and soil/vegetation heat and moisture flux algorithms can be used jointly to retrieve higher-level products such as subsurface soil moisture and temperature profiles, and surface heat fluxes. These approaches require significant development before they can be applied practically on a large-scale basis.

III. Algorithm Description

A. Emission Model and Sensitivities

The retrieval algorithm for m_e, w_e, and T_e is based on a radiative transfer (RT) model which relates parameters describing the surface and atmosphere to the observed brightness temperatures. The model represents these processes in a simplified form appropriate to the spatial scale of the satellite footprints. The parameterization of the model is designed with the retrieval algorithm in mind. Errors in the model approximations, and a-priori uncertainties in the model parameters, will be reflected in the resulting retrieval errors. These errors and uncertainties can be estimated, and their influences on retrieval error evaluated.

Various elements of the RT model used here have been reported elsewhere [8], [1 5], [30]. However, some aspects of the model are new, hence the model equations with brief descriptions are provided here in the Appendix. We write the satellite-observed brightness temperature as:

$$T_{B_i} = \Phi_i(\mathbf{x}) \tag{1}$$

where, the model function Φ_i (x) relates the parameters $x = \{x_j\}$ of the soil-vegetation-atmosphere medium to the brightness temperature observations, T_{B_i}, at channel *i*. The RT model parameters are listed in Table 2.. The parameters are grouped into two categories: (a) parameters defining media and sensor characteristics or empirical relationships, and (b) retrievable geophysical variables. The atmospheric variables are included in the retrievable list although the sensitivity of brightness temperature to these variables over land, at frequencies below 37 GHz, is too low to afford reliable retrievals. (Retrieval of water vapor and cloud liquid water by including the 21-23 and 37 GHz frequencies may be possible over surfaces of low variability, particularly if ancillary data are available to characterize the background surface emissivity.) The soil and vegetation temperatures are retrieved as a single surface effective temperature, T_e, averaged over the satellite footprint. Similarly, m_e and w_e represent effective values averaged over the footprint. The model assumes that all radiometer channels are coincident and have the

same footprint. (This is expected to be accomplished in the AMSR case by preprocessing of the brightness temperature data,)

Figure 1 shows the computed brightness temperatures, T_B, at 6.6, 10.7, and 18 GHz, vertical and horizontal polarizations, at θ = 50.3° (i.e. the SMMR observing characteristics). The curves are shown as functions of m_e, w_e, T_e, q_v, and q_l, for a standard atmosphere, and nominal values, except where each variable is varied, of m_e = 0.1 g cm^{-3}, w_e = O kg m^{-2}, T_e = 30 C, q_v = 2.5 cm, and q_l = O mm. The sensitivity of brightness temperature to moisture and vegetation is greater at H than at V polarization, while the converse is true for temperature. The sensitivity to moisture decreases, while the sensitivity to vegetation increases, with increasing frequency. The sensitivity decreases with increasing vegetation, and there is little sensitivity at vegetation water contents greater than -1.5 kg m^{-2} even at 6.6 GHz (Figure l(b)). Thus, it is unlikely that retrievals of soil moisture will be feasible at vegetation amounts beyond this threshold. The different sensitivity of brightness temperature to m_e, w_e, and T_e, as a function of frequency and polarization, is the basis for the ability to independently retrieve these parameters using a multichannel algorithm. At these frequencies, the sensitivity to cloud liquid water is minimal, as is also the case with water vapor, except at the 18H channel.

The sensitivities can be computed explicitly. It is convenient to normalize the sensitivities such that the sensitivity, S_{ij}, of brightness temperature at channel i to geophysical parameter x_j is expressed as:

$$S_{ij} = \left| X_j \left(\frac{\partial \Phi_i}{\partial x_j} \right)_{\mathbf{x} = \mathbf{x}_o} \right| \qquad (2)$$

where, X_j are typical parameter dynamic ranges, and $\mathbf{x}_o$ are baseline values of the parameters, x, at which the sensitivities are evaluated. Normalized sensitivities indicate more clearly the relative magnitudes of the sensitivities to the different parametrs, in Kelvins. The sensitivities are shown in Table 3 for horizontal and vertical polarizations at 6.6 GHz for two cases-–for bare soil and

for vegetation water content of 1.5 kg m^{-2} (spanning the range of vegetation conditions under which soil moisture retrievals using SMMR or AMSR are likely to be feasible). The sensitivities to moisture and vegetation are clearly much reduced for the higher vegetation level, although the sensitivity to surface temperature remains high. Thus, accurate retrieval of surface temperature can be achieved regardless of vegetation cover, and only the interpretation of the surface temperature (i.e. soil or vegetation) will change. Sensitivities to other variables (e.g atmospheric water vapor and liquid water) and model parameters (e.g. uncertainties in roughness or vegetation albedos) are typically an order of magnitude or so less than to the three main variables (m_e, w_e, and T_e), and hence are not dominant factors in the retrievals.

B. Retrieval Procedure

Retrievals of land surface parameters using passive microwaves have, in the past, used mainly surface classification and linear-regression methods. Nonlinear algorithms (iterative and neural-network) have also been used, particularly to improve retrievals where the physics of the radiative-transfer and interaction processes are nonlinear [32], [33]. Bayesian estimation techniques have also been investigated to include, optimally, a-priori information on sensor noise, model uncertainties, probability distributions of the parameters being estimated, and ancillary data from ground truth or other sensors [34]. In this paper we use an iterative least-squares minimization algorithm.

The algorithm retrieves, simultaneously, M geophysical variables (j = 1 to M) from measurements at N brightness temperature channels (i = 1 to N), where N should be greater than M for stable retrievals. Initially, to evaluate the procedure, we have used N = 6, which for the SMMR case includes the six lowest-frequency channels: 6.6H, 6.6V, 10.7H, 10.7V, 18H, and 18V. The three primary variables, m_e, w_e, and T_e, are included in the retrieval set, and also precipitable water, q_v, i.e. M = 4. (The inclusion of q_v is for illustration only, and is intended to show the difficulty of retrieving this parameter over land at low frequencies.) The procedure finds values for the set of variables x = $\{m_e, w_e, T_e, q_v\}$ that minimize χ^2, i.e. the weighted-sum

of squared differences between observed, $T_{B_i}^{obs}$, and computed, Φ_i (x), brightness temperatures, where:

$$\chi^2 = \sum_{i=1}^{6} \left(\frac{T_{B_i}^{obs} - \Phi_i(\mathbf{x})}{\sigma_i} \right)^2 \qquad (3)$$

The efficient Levenberg-Marquardt algorithm is used to search for the set of variables, x*, that minimizes the χ^2 [35]. At each retrieval point, the algorithm starts with a-priori values, $\mathbf{x_0}$, of the geophysical variables to be retrieved, and adjusts these iterative y until convergence to the minimum χ^2 is achieved within specified criteria, The σ_i represents the measurement noise standard deviation in channel *i.* The model parameter values used in computing Φ_i (x) are as described in the Appendix.

The model, Φ_i (x), is mathematically well-behaved, hence convergence of the retrieval algorithm is normally straightforward, except where the model cannot adequately represent the surface emission (e.g. where snow or open water occur in the footprint), or where the sensitivities to the parameters are too low. In such cases the parameter values retrieved by the algorithm are unreliable, as indicated by high values of the minimized χ^2.

C. Retrieval Simulations

Simulations have been performed to estimate the accuracy of the retrieval algorithm in the presence of sensor noise. The variables to be estimated, $\mathrm{x} = \{m_e, w_e, T_e, q_v\}$ were simulated as sets of 200 uniform random variables (i.e. number of realizations, $n_r = 200$) spanning the dynamic ranges: m_e = 0.03 to 0.35 g cm^{-3}; w_e = O to 1.5 kg m^{-2}; T_e = O to 40 “C; and q_v = 1 to 5 cm. From these distributions, model brightness temperatures, $T_{B_i} = \Phi_i(\mathbf{x})$, were computed for the six SMMR channels to be used in the retrieval. To these brightness temperatures, gaussian random noise of $AT = 0.3$ K (1σ) was added to simulate noisy SMMR observations. The retrieval algorithm was then applied to these simulated observations, $T_{B_i}^{obs}$, and parameter estimates x* obtained. Starting values of $\mathbf{x_0}$ = {0.05, O, 0, 1} were used, and a maximum of N_{iter} = 10

iterations was allowed, which was found to be sufficient for convergence. Fig 2 shows scatterplots of the 'retrieved' versus 'true' parameters obtained in this manner for one set of n_r = 200 realizations, with ΔT = 0.3 K. Precipitable water is not well retrieved, as expected, although there is some sensitivity. Negative retrieved values of q_v are set to zero in the algorithm. Figure 3 shows histograms of the retrieval errors, E = $\mathbf{x}^*$ - x, for the same set of realizations and noise ΔT' value as Figure 2. (The horizontal scales of the histograms in Figure 3 are normalized to the parameter ranges.) The means and standard deviations of the simulated retrieval errors, ε, are given in Table 4. The values shown in Table 4 are averages over 10 different sets (n_r = 200) of ΔT= 0.3 K sensor noise realizations, to improve the reliability of the retrieval error estimates. Also shown in Table 4 are the retrieval error estimates for an increased sensor noise of ΔT = 0.5 K. The means of the retrieval errors are not significantly different from zero, indicating that the retrieval algorithm is unbiased. The standard deviations of the retrieval errors for ΔT= = 0.3 K are approximately 60% less than for ΔT= 0.5 K, as expected based on the ratio between the sensor noise values.

Figure *2* and Table 4 provide statistics for the simulated retrievals over the full dynamic ranges of all variables. To illustrate how the retrieval accuracy varies as a function of each variable, we compute the retrievals in similar fashion to the above, for ΔT = 0.3 K, but this time each of the variables in turn is varied discretely in 20 steps over its range, while the other variables are varied randomly over their ranges. The results are shown in Figure 4. Panels (a) through (d) show the soil moisture retrieval error means and standard deviations as functions of m_e, w_e, T_e, and q_v respectively. Similarly, panels (e) through (h), (i) through (l), and (m) through (p) show the retrieval errors for vegetation water content, surface temperature, and precipitable water. The solid lines are the means, and the dashed lines the standard deviations, of the errors. In general, the mean errors are all close to zero indicating that the retrievals are unbiased over the full ranges of variability. The slight wiggliness of the lines is the statistical uncertainty of estimating the mean errors using n_r = *200* realizations. (This uncertainty decreases as n_r increases. Using a larger value of n_r does not provide additional insight into the main results of

Figure 4 however.) As shown in Figure 4, the retrieval error standard deviations are not very sensitive to T_e and q_v, except for ε_q which has a broad peak with a maximum near T_e = 14 C. Within the surface temperature range corresponding to this peak, for the conditions of our simulation, the background surface brightness temperature is similar to the tropospheric water vapor emitting temperature, and hence there is little sensitivity of the satellite-observed brightness temperature to the water vapor. This points out the difficulty of retrieving water vapor (or cloud liquid water) over land, except where the land brightness temperature is much lower, or higher than the tropospheric water vapor (or cloud) emitting temperature.

A significant feature of Figure 4 is the increase in error standard deviations ε_m and ε_w with increase in vegetation water content (panels (b) and (f)). This is expected, due to the masking of the underlying soil, and the saturation of vegetation emission, at the higher vegetation amounts, at frequencies of 6.6 GHz and above. There is little potential for using the SMMR (or AMSR) for retrieval of m_e or w_e at values of w_e > -1.5 kg m^{-2}. At vegetation amounts below --0.2 kg m^{-2} (approaching bare soil) the surface temperature retrieval error, ε_T, increases markedly (panel (j). For bare soils, the algorithm has difficulty discriminating between the effects of increasing T_e and decreasing *me* on the brightness temperature (note the corresponding increase in ε_m in panel (b)). This implies that for bare soils, surface temperature may not be retrievable accurately using microwave data alone, and ancillary surface temperature information from other sources (satellite or in situ) may be useful in improving the retrievals of soil moisture over bare soils.

IV. Application to SMMR Data

The simulation results (Figure 4) indicate that, even accounting for modeling errors (which we have not simulated here), retrieval accuracies for m_e, w_e, and T_e of better than 0.06 g cm^{-3}, 0.1 kg m^{-2}, and 2 C, respectively, should be feasible using satellite instruments such as the S MMR and AMSR over a wide range of conditions, provided the footprint-averaged vegetation water content is less than about 1.5 kg m^{-2}. No externally-provided data from other sensors or model-generated

output, such as surface temperature or atmospheric moisture data, are assumed. The idealized RT model used in the simulations does not account for nonlinearities caused by sub-pixel surface heterogeneity, variability in surface topography and roughness, or uncertainties in model parameters. Thus, it is important to test the retrieval algorithm using actual satellite data, under conditions in which the performance can be readily assessed. For this purpose, we have run the algorithm using four years of Nimbus-7 SMMR data over a 4° x 10° latitude-longitude region of the African Sahel, between 12° to 16°N, and 0° to 10°E, Figure 5. In this region there are strong seasonal signals of moisture, vegetation, and temperature, related to the precipitation cycle between the rainy and dry seasons. The region is devoid of large-scale topography, and the surface can be viewed as relatively homogeneous at the large scale (-50-150 km) of the SMMR footprints. The region is a fragile ecosystem, and hence is also of scientific and sociological interest due to the ongoing threat of drought and desertification.

The SMMR data are derived from the reprocessed SMMR brightness temperature data set available from the NSIDC DAAC [36]. For this study, these data have been binned separately for daytime and nighttime passes (ascending and descending orbits, respectively) onto 6-day and monthly, 1/2° x 1/2° lat-lon grids, for ease of data handling and comparison with other data sets. The retrieval algorithm was applied to the monthly, daytime binned data; thus the geophysical parameter estimates are also at the monthly, 1 /2° grid scale. Retrievals were done on the monthly, 1/2° grid data to expedite analysis over the 4-year time span for this study, however future retrievals will be performed on the swath data prior to binning, to avoid the temporal and spatial averaging that occurs using binned data. Daytime data were used since there are extensive gaps in the nighttime data near the equator due to the alternate-day on-off operation of the sensor (the on-off switching was done at the descending-node equator crossing near local midnight).

A. Model Calibration

Uncertainty in the absolute calibration of the SMMR brightness temperatures, and in some of the RT model parameters, requires that the retrieval model first be ‘calibrated’ to the S MMR

observations. This is done by selecting two homogeneous sites, one in the desert and one in tropical forest, where offsets in the brightness temperatures at the various channels can be determined and the model parameters, h, Q, and ω_p, fine-tuned. These sites are marked on Figure 5 as points 'A' and '13', respectively. Since the roughness characteristics of desert, and the single scattering albedo of tropical forest, are not expected to change significantly with time, the parameters, h, Q, and ω_p, are determined once, and then held constant in the temporal application of the algorithm. They were also held constant spatially in this study. In future work, the spatial dependence of these parameters will be investigated to improve the algorithm performance.

Desert:

Over the desert site, with an assumption of no vegetation ($\tau_c \rightarrow 0$), the RT model equations (see Appendix) can be rearranged to express the soil reflectivity as a function of the observed brightness temperature, surface temperature, and atmospheric absorption and emission:

$$r_{s_p} = \frac{T_{B_p} - T_u - T_d \exp(-\tau_a)}{\exp(-\tau_a)\left\{T_d + T_{sky} \exp(-\tau_a)\right\}} \qquad (4)$$

Climatological estimates of q_v, T_{ae}, and T_e, and S M M R brightness temperatures, were used to evaluate r_{s_h} and r_{s_v} at the desert site (assuming cloud-free conditions) according to Equation (4). Using Equations (A. 1), (A.2), (A. 12), and (A. 13), and assuming dielectric properties of a dry, sandy soil, values for h and Q were obtained for each frequency. These are given in Table 5.

Forest:

Over the forest site, the high vegetation opacity masks the underlying soil. Using the limit $\tau_c \rightarrow$ large, we can rearrange the RT model equations to express the vegetation single-scattering albedo as a function of the observed brightness temperature, surface temperature, and atmospheric absorption and emission:

$$\omega_p = 1 - \frac{(T_{B_p} - T_u)}{T_e \exp(-\tau_a)} \tag{5}$$

Using climatological and SMMR data over the forest site, as for the desert site, we obtain values for ω_p at each frequency and polarization as given in Table 5. Cloud effects are ignored in this calibration, since they are expected to be small at 6 to 18 GHz according to Figure 1.

The values of h and Q obtained are consistent with values obtained from previous ground-based field experiments [37], [38]. Similarly, the values obtained for ω_h and ω_v are physically reasonable and within their expected ranges [39]. It should be remembered, however, that by matching the RT model to the SMMR observations at the calibration sites we have essentially lumped any brightness temperature calibration offsets into the derived values of h, Q, and ω_p. It is difficult to distinguish radiometer absolute calibration offsets from model offsets without more extensive analysis, and for our purposes here it is not necessary to do so. Fine-tuning a global algorithm will require this to be done, however. obtaining physically reasonable values for the parameters in Table 5 gives credence to the RT mode], and also to the good relative calibration of the SMMR data. In future investigations this calibration procedure will be performed using an optimum statistical method, using globally-distributed sites and available in-situ and land-atmosphere model output data instead of climatology. Fine-tuning of the vegetation opacity coefficient, b, can also be done using the SMMR data by estimation over large-area homogeneous sites of known biomass. Instrumented sites of this kind are not currently available, however; hence in this study we use the form for b derived from ground-based measurements, as described in the Appendix.

B. Retrieval Results

Figure 6(a) shows a time-series of the SMMR-derived geophysical parameters, retrieved on the 1/2° grid, and further averaged over the region shown in Figure 5. Superimposed on the plot is the precipitation rate, averaged over the same region, obtained from an operational forecast model product of the National Centers for Environmental Prediction (NCEP). Figure 6(b) shows

comparisons between the SMMR retrievals of m_e and T_e and the NCEP model outputs of soil wetness and surface temperature. The variables in Figure *6* have been scaled as indicated, to have similar dynamic ranges on the plots. The NCEP model output products are part of a 13-year (1982-94) operational forecast model reanalysis project [40]. The products are generated as outputs of a 6-hourly data-assimilation and forecast cycle, and the products shown here were obtained from NCEP as monthly-averages on a 2.5° x 2.5° grid, and then averaged over the area shown in Figure 5. The model output data cannot be considered as "truth", but they represent self-consistency in the forecast model as related to the in-situ data used in the most recent (6-hourly) data assimilation. Thus, the data are valuable for comparing against the temporal trends of the SMMR retrievals.

Figure 6(b) clearly demonstrates the ability to retrieve soil moisture and temperature from the SMMR with the correct seasonal cycle. It is difficult to compare quantitatively the absolute values of the SMMR retrievals and the NCEP data, since the NCEP soil wetness represents an average value over the top 10 cm, as compared to the top few mm for the SM M R. Thus, the SMMR derived values of soil moisture are more than a factor of four lower than the NCEP values. Also, the NCEP surface temperature is a skin surface value, as compared to the top few cm for the SMMR. In addition, the SMMR data are samples near 12 noon local time, while the NCEP data are averages over the diurnal cycle. It is interesting to note the dip in the SMMR-retrieved surface temperatures (Figure 6(a)) that appear to coincide with the peaks of the NCEP rain estimates. These dips are less pronounced in the NCEP temperatures (Figure 6(b)), but are visible as plateaus on the decreasing side of the curves. Normally, under moist conditions the soil temperature is cooler than for a dry soil, due to the increased evaporation from the soil and the soil thermal inertia. This cooling effect is more pronounced in the SMM R data sampled near local noon than for the diurnally-averaged NCEP data.

Figure 7 shows scatterplots of the SMMR-derived and NCEP model output variables shown in Figure *6(b).* The best fit regression lines are also shown. The standard deviation of the

temperature comparisons in Figure 6(b) is 2.7 C. It must be remembered that different quantities are being compared between the remotely-sensed and model output data, and the data represent monthly averages, over a relatively large 4° x 10° area. Nevertheless, the level of agreement is very good. Better agreement is to be expected when the comparisons can be carried out at shorter time scales, such that the moisture and temperature variations can be tracked more accurately, and where the accuracy of the comparison data can be better verified. The Sahel is a region where the accuracy of the operational forecast models is suspect, due to the sparseness of in situ meteorological data for initializing the forecasts.

5. Discussion

In this study we have shown via simulations that surface soil moisture, vegetation water content, and surface temperature are retrievable with useful accuracies using passive microwave measurements at 6 to 18 GHz. Several caveats in the physical model have been pointed out, however, that may decrease the retrieval accuracies in practical applications. The same algorithm as used in the simulations has been applied to historical SMMR data, to investigate the retrievability of these variables using actual satellite data in a region of low vegetation. Comparisons of the SMMR retrievals with forecast model reanalysis data, over a region in the African Sahel, on a monthly time scale, are very encouraging. Subsequent work is required to extend these results to other regions, and to validate the retrievals more quantitatively. This can be done in conjunction with some of the large-scale data production and validation exercises currently underway for land-atmosphere interaction modeling [e.g. 41]. Trade-offs in retrieval algorithm design also need to be investigated. In this study, the 18 GHz channels were included in the algorithm for their anticipated greater sensitivity to vegetation at low levels, and for better temperature sensitivity and stability. However, the 6.6 and 10.7 GHz channels may suffice for this purpose, and the 18 GHz channels may in fact add more noise than information over heterogeneous regions, since the footprint size at 18 GHz is a factor of 2 to 3 smaller than at 6.6

GHz. (Pre-processing of the brightness temperatures to the same footprint sizes helps reduce this problem.) The use of algorithms based on brightness temperature polarization ratios as a means for removing surface temperature dependence also needs to be investigated.

6. Appendix: Microwave Emission Model

A. Bare Soils

For a homogeneous soil with a smooth surface, the reflectivities at vertical and horizontal polarizations, r_{o_v} and r_{o_h}, are given by the Fresnel expressions:

$$r_{o_v} = \left| \frac{\varepsilon_r \cos\theta - \sqrt{\varepsilon_r - \sin^2\theta}}{\varepsilon_r \cos\theta + \sqrt{\varepsilon_r - \sin^2\theta}} \right|^2 \tag{A1}$$

$$r_{o_h} = \left| \frac{\cos\theta - \sqrt{\varepsilon_r - \sin^2\theta}}{\cos\theta + \sqrt{\varepsilon_r - \sin^2\theta}} \right|^2 \tag{A.2}$$

where, θ is the incidence angle (relative to the surface normal), and ε_r *is* the complex dielectric constant of the soil which depends primarily on the soil moisture content, m. The soil is considered as a mixture of soil particles and pore spaces filled with air and water [42], [43]. The dielectric model used here is that of Dobson et al. [43], and requires the specification of the sand and clay mass fractionss and c (which describe the soil texture) and the soil bulk density ρ_b. In this study, a value of ρ_b = 1.4 g cm^{-3} is used, ands and c are given values typical of a sandy soil. For global applications, a soils database can be used to estimate the large-scale soil texture [e.g. 44]. The smooth-surface emissivity, e_{o_p}, is related to the reflectivity, r_{o_p}, by reciprocity:

$$e_{o_p} = 1 - r_{o_p} \tag{A.3}$$

where, the subscript denotes either vertical or horizontal polarization ($p = v$ or h). For a soil with uniform temperature, T_s, the soil brightness temperature, T_{bs_p}, is given by:

$$T_{bs_p} = e_{o_p} T_s \tag{A.4}$$

Under natural conditions, the soil temperature has a nonuniform, time-varying, vertical profile determined by the net heat flux at the surface and the soil thermal properties. The moisture profile is also nonuniform and time-varying, determined primarily by the net moisture flux at the surface (precipitation minus evaporation) and the hydraulic properties of the soil. The soil temperature and moisture profile dynamics are coupled, since soil thermal properties are moisture dependent. (Since the soil heat and moisture flux models provide time-dependent information and constraints on the variability of the moisture and temperature profiles, these models and information can potentially be incorporated into the retrieval algorithms to provide improved soil moisture and temperature estimates.)

For nonuniform temperature and moisture profiles, the dependence of the soil brightness temperature, T_{bs_p}, on subsurface variability of temperature, $T_s(z)$, and moisture, m(z), is expressed as:

$$T_{b\,s_p} = \int_{-\infty}^{0} T_S(z) F_p\{\varepsilon_r(z)\}\, dz \tag{A.5}$$

where, z is the vertical distance above the surface (positive in the upward direction). The form of $F_p\{\varepsilon_r(z)\}$ can be detertnined accurately using a coherent radiative transfer approach [45].

Approximate Form:

An approximate form for $F_p\{\varepsilon_r(z)\}$, valid when the moisture profile does not vary rapidly over the depth of a wavelength in the medium (the wavelength in the medium varies with dielectric constant and hence also with depth), is obtainable using an incoherent radiative transfer approach, which leads to an expression equivalent to (A.5):

$$T_{bs_p} = (1 - r_{o_p})\, T_{se} \tag{A.6}$$

$$T_{se} = \int_{-\infty}^{0} T_s(z)\, \widetilde{F}_{N_p}\{\varepsilon_r(z)\}\, dz \qquad (A.7)$$

where, r_{o_p} now denotes the Fresnel reflectivity of a homogeneous soil of dielectric constant $\varepsilon_r(0)$, T_{se} is the soil "effective temperature", and $\widetilde{F}_{N_p}\{\varepsilon_r(z)\}$ is an approximation of $F_p\{E,(z)\}$, normalized to an integral of unity:

$$\widetilde{F}_{N_p}\{\varepsilon_r(z)\} = a(z)\ \mathrm{Cxp}\left(-\int_z^0 \alpha(z')\, dz'\right) \qquad (A.8)$$

$$\alpha(z) = 2\, Im\left\{\frac{2\pi}{\lambda}\sqrt{\varepsilon_r(z) - \sin^2\theta}\right\} \qquad (A.9)$$

and where λ is the wavelength in air. Equations (A.6)–(A.9) can be derived directly as a first-order approximation to Equation (A.5), and express the fact that, to first order, the reflectivity (and emissivity) of a soil is determined by the dielectric constant (and hence the soil moisture) at the soil surface (z = O), while the brightness temperature is affected by the subsurface temperature and moisture profiles. This approximation is convenient, since Equation (A.6) has a simple form equivalent to Equation (A.4). As the wavelength increases, the approximation becomes less accurate since the emissivity becomes dependent not j ust on the surface dielectric constant but on the subsurface gradient of the dielectric constant. However, it is a valid approximation provided the emissivity is considered to be representative of the average or "effective" moisture, m_e, within a top soil layer of depth d_m, the "moisture sensing depth", where d_m depends on wavelength. Simulations have shown [46] that d_m is about a tenth of a wavelength in the medium. Thus, d_m is a variable that itself depends on the soil moisture content. The longest SMMR wavelength is 4.3 cm, and for a dry soil the wavelength in the medium will be about half this value. Thus, we find for SMMR (or AMSR) that $d_m < 2$ mm.

For uniform soil moisture (i.e. uniform dielectric constant), and **nadir-viewing,** $\widetilde{F}_{N_p}\{\varepsilon_r(z)\}$ takes the simple form:

$$\tilde{F}_{N_p}\{\varepsilon_r(z)\} = \alpha \exp(\alpha z) \tag{A.10}$$

$$\alpha = \frac{4\pi n''}{\lambda} \tag{A.11}$$

where n'' is the imaginary part of the refractive index (square root of the dielectric constant), i.e. $n'' = Im\{\sqrt{\varepsilon_r}\}$. The "temperature sensing depth", d, = a^{-1}, *is* defined as the depth of the surface layer from which ~63% of the emitted radiation originates. Alternatively, d_t is the distance in the medium over which the intensity of transmitted radiation decreases by a factor of $e^{-1} = 0.368$ (for a medium of uniform temperature and moisture), thus d_t *is* also commonly referred to as the "penetration depth" in the medium. In summary, the sensing depths d_m and d_t define the approximate soil depths over which the soil moisture influences the emissivity, and the soil moisture and temperature together influence the effective temperature, respectively. These parameters are useful in describing the characteristics of microwave emission from soils.

B. Rough Surface

The expressions for reflectivity (Equations (A. 1) and (A.2)) must be modified for rough surfaces, to take into account the effects of surface scattering. Theoretical expressions for reflectivity have been developed using statistical parameters such as height standard deviation and horizontal correlation length to characterize the surface [4'7]. Although these provide insight into the scattering mechanisms, the expressions are not easy to apply in practice since they require knowledge of the soil surface height and slope statistics, and are computationally intensive.

A simpler, semi-empirical formulation was proposed [37] which also uses two parameters to characterize the surface: a height parameter h (which is related to the height standard deviation), and a polarization mixing parameter Q. In this formulation, the rough surface reflectivity, r_{s_p}, is related to that of a smooth soil, r_{o_p}, by:

$$r_{s_v} = [(1 - Q)\, r_{o_v} + Q\, r_{o_h}] \exp(-h) \tag{A.12}$$

$$r_{s_h} = [\,(1 - Q)\, r_{o_h} + Q\, r_{o_v}\,] \exp\,(-h) \tag{A.13}$$

The available experimental database is too limited to derive reliable expressions for the frequency and viewing angle dependence of *h* and Q. For analysis of data at 1.4 GHz, a value of zero is often assigned to Q, and roughness is expressed by a value between O and 0.3 for *h* [48]. This formulation cannot represent fully the varieties of roughness present in nature, but captures in simplified form, and with few parameters, the major phenomenological and observable roughness effects on microwave brightness. In the retrieval simulations (Section III.C) we set $h = 0.1$, and Q = O. In the SMMR retrievals (Section IV), the parameters *h* and Q are estimated as calibration parameters. With these modifications for the surface reflectivity, the surface brightness temperature, from Equation (A.6), becomes:

$$T_{bs_p} = (1 - r_{s_p})\, T_{se} \tag{A.14}$$

C. Vegetation

Vegetation is represented as a single-scattering layer above a rough soil. The soil moisture and temperature may vary with depth. However, the soil characteristics—texture, hydraulic and thermal properties, etc.—are considered uniform with depth. The brightness temperature at the top of the vegetation layer T_{b_p} can be written as a function of soil brightness temperature T_{bs_p}, soil reflectivity r_{s_p}, vegetation opacity τ_c, vegetation single-scattering albedo ω_p, and vegetation effective temperature *Tee*, as [15], [30]:

$$T_{b_p} = T_{bs_p} \exp(-\tau_c) + T_{ce}\,(1 - \omega_p)\,[1 - \exp(-\tau_c)]\,[1 + r_{s_p} \exp(-\tau_c)] \tag{A.15}$$

The reflectivity r_p of the two-layer soil/vegetation surface is a function of the soil reflectivity r_{s_p}, and vegetation opacity τ_c:

$$r_p = r_{s_p} \exp\,(-2\tau_c) \tag{A.16}$$

The term "effective temperature" for soil and vegetation emphasizes that when the physical temperatures of the media are nonuniform the effective temperatures in the radiative transfer

expressions are weighted means of the actual temperatures. For our retrieval model we assume for simplicity that the medium is homogeneous with temperature T_e (so that $T_{se} = T_{ce} = T_e$), and Equations (A. 14) and (A. 15) are combined to give:

$$T_{b_p} = T_e \{ (1 - r_{s_p}) \exp(-\tau_c) + (1 - \omega_p) [1 - \exp(-\tau_c)] [1 + r_{s_p} \exp(-\tau_c)] \} \qquad (A.17)$$

In Equation (A. 17) the single scattering albedo has a polarization dependence since the scattering depends on the relative orientations of leaves, stalks, and branches within the vegetation volume [49]. The opacity τ_c may also exhibit a polarization dependence, but there is little evidence to show that this is of comparable significance to the other modeled effects. The dependence of τ_c on vegetation columnar water content WC, follows an approximately linear relationship which may be written as:

$$\tau_c = b \quad w_c / \cos\theta \qquad (A.18)$$

The $\cos\theta$ factor accounts for the slant observation path through the vegetation, and *b* is a parameter that depends weakly on vegetation type at low frequencies. Experimental data indicates that *b* is approximately proportional to frequency and has a value of -0.1 at 1.4 GHz [50]. Recent studies indicate, however, that as frequency increases the frequency dependence of *b* decreases, and its dependence on canopy structure increases [51], [52]. Thus, information on vegetation type will most likely be necessary to calibrate the parameter *b* for global applications. The single-scattering albedo ω_p may also exhibit a dependence on vegetation water content, but the effect of this on brightness temperature is expected to be small compared to the effect on τ_c and is not modeled. In the retrieval simulations (Section 111. C), ω_p is set equal to zero, but it is estimated as a calibration parameter in the SMMR retrievals (Section IV).

Heterogeneity:

For a heterogeneous scene, Equation (A. 14) must be interpreted in the sense that the parameters and terms represent area-weighted averages over the scene components within the observed footprint. The footprint spatial dimension is defined by the antenna pattern. If we

consider a simple representation in which the antenna pattern is constant within the footprint area, and zero outside, then the observed brightness temperature T_b is an area-average of the component brightness temperatures T_{b_j} within the footprint, i.e.

$$T_b = \sum_{j=1}^{N} f_j T_{b_j} \tag{A.19}$$

where, f_j are the fractional coverages of N distinct surface types within the footprint (the f_j sum to unity).

An analysis has been done [27] to investigate the differences between estimates of area-averaged geophysical variables retrieved from area-averaged brightnesses T_b, and direct area-averages of the geophysical variables over the footprint. These differences are caused by nonlinearities in the microwave model, such as caused by vegetation. Simulations show that the differences are small, except in situations where large contrasts occur within the footprint between roughly equal fractions of bare soil and dense vegetation. Such cases should be identified and interpreted carefully in the retrievals. In our retrieval model we assume that the vegetation is homogeneously distributed over the footprint. Thus, in Equation (A. 18) the vegetation water content is understood to be an "effective" value, w_e, averaged over the footprint.

D. Atmosphere

The microwave brightness temperature, T_{B_p}, observed by a spaceborne radiometer above the atmosphere is:

$$T_{B_p} = T_u + \exp(-\tau_a)[T_{b_p} + r_p \{ T_d + T_{sky} \exp(-\tau_a) \} 1 \tag{A.20}$$

where, T_u and T_d *are* the upwelling and downwelling atmospheric radiation, T_{skv} is the space background brightness (2.7 K), τ_a is the atmospheric opacity, r_p is the surface reflectivity, and T_{b_p} *is* the surface brightness temperature (Equation (A. 17)). For low atmospheric absorption (as

is the case at 6 to 18 GHz), T_u and T_d *can be* expressed using the effective radiating temperature approximation:

$$T_u \cong T_d \cong T_{ae}[1 - \exp(-\tau_a)] \tag{A.21}$$

where, T_{ae} is the weighted-mean temperature of the microwave-absorbing region of the atmosphere. T_{ae} is frequency dependent, and depends also on the vertical distributions of atmospheric temperature, humidity, and liquid water. The dependence of T_{ae} on atmospheric profile variability is small, and T_{ae} may be expressed simply as a function of the surface air temperature T_{as} and a frequency-dependent offset δT_a:

$$T_{ae} \cong T_{as} - \delta T_a \tag{A.22}$$

Values for δT_a *are* obtained from calculations using model or climatological atmospheric data [40], [53].

The opacity τ_a along the slant-range atmospheric path is dependent on the viewing angle θ and the vertical-column amounts of water vapor q., and cloud liquid water q_l, and can be written (for a plane parallel atmosphere) as:

$$\tau_a = (\tau_o + a_v q_v + a_l q_l) / \cos\theta \tag{A.23}$$

where, τ_o is the nadir oxygen opacity, and a_v and a_l *are* the water vapor and cloud liquid water nadir opacity coefficients, respectively. Values of these parameters are derived from the standard equations of gaseous and water-droplet absorption in the atmosphere (Rayleigh absorption is assumed for the cloud droplets).

E. Summary

In the above discussion we have described how, in order to reduce the parametrization of the microwave model to a convenient set of three dominant surface variables, we have assumed homogeneous conditions such that the retrieved parameters represent effective values averaged

over the radiometer footprint. Information on sub-footprint variability is not obtainable from the footprint-averaged retrievals. The retrieved variables are thus defined as follows:

m_e : Area-averaged mean moisture in the top few mm of soil.

we : Area-averaged water content in the vertical column of vegetation overlying the soil.

T_e : Area-averaged mean microwave radiating temperature of the surface.

7. ACKNOWLEDGEMENTS

This work was carried out at the Jet Propulsion Laboratory, California Institute of Technology, under contract to the National Aeronautics and Space Administration.

8. REFERENCES

[1] J. Shukla and Y. Mintz, "Influence of land-surface evapotranspiration on the Earth's climate," *Science,* vol. *215,* pp. 1498-1500, 1982.

[2] T. Delworth and S. Manabe, "The influence of soil wetness on near-surface atmospheric variability," *J. Climate, vol. 2,* pp. 1447-1462, 1989.

[3] K. L.. Brubaker and D. Entekhabi, "Analysis of feedback mechanisms in land-atmosphere interaction," *Water Resour. Res.,* vol. 32, pp. 1343-1357, 1996.

[4] A. C. M. Beljaars, P. Viterbo, M. J. Miller, and A. J. Betts, "The anomalous rainfall over the United States during July 1993: Sensitivity to land surface parametrization and soil moisture anomalies," Mon. *Wea. Rev., vol. 124,* pp. 362-383, 1996.

[5] MTPE, *"Mission To Planet Earth Science Research Plan,"* Office of Mission To Planet Earth, National Aeronautics and Space Administration, Washington, DC, 1996.

[6] P. Gloersen, D. J. Cavalieri, A. T. C. Chang, T. T. Wilheit, W. J. Campbell, O. M. Johannessen, K. B. Katsaros, K. F. Kunzi, D. B. Ross, D. Staelin, E. P. L. Windsor, F. T. Barath, P. Gudmansen, E. Langham, and R. Ramseier, "A summary of results from the first Nimbus-7 SMMR observations," *J. Geophys. Res., vol.* 89, pp. 5335-5344, 1984.

[7] J. P. Hollinger, J. L. Pierce, and G. A. Poe, "SSM/I instrument evaluation," *IEEE Trans Geosci. Rem. Sens.,*. vol. 28, pp. 781-790, 1990.

[8] E. G. Njoku and D. Entekhabi, "Passive microwave remote sensing of soil moisture," *J. Hydrology*, vol. 184, pp. 101-129, 1996.

[9] M.-Y. Wei (Ed.), "Soil moisture: Report of a workshop held in Tiburon, CA, 25-27 January 1994," *NASA Conference Publication #3319*, National Aeronautics and Space Administration, Washington, DC, 1995.

[10] J. M. Norman and F. Becker, "Terminology in thermal infrared remote sensing of natural surfaces," *Rem. Sens. Rev.*, vol. 12, pp. 159-173, 1995.

[11] J. R. Wang, "Effect of vegetation on soil moisture sensing observed from orbiting microwave radiometers," *Rem. Sens. Environ.*, vol. 17, pp. 141-151, 1985.

[12] E. G. Njoku and 1. R. Patel, "Observations of the seasonal variability of soil moisture and vegetation cover over Africa using satellite microwave radiometry," *Proc. ISLSCP Conference, Rome, Italy, 2-6 December 1985*, ESA SP-248, European Space Agency, Paris, France, 1986.

[13] M. Owe, A. Chang, and R. E. Golus, "Estimating surface soil moisture from satellite microwave measurements and a satellite-derived vegetation index," *Rem. Sens. Environ.*, vol. 24, pp. 131-345, 1988.

[14] B. J. Choudhury and R. E. Golus, "Estimating soil wetness using satellite data," *Int. J. Rem. Sens.*, vol. 9, pp. 1251-1257, 1988.

[15] Y. H. Kerr and E. G. Njoku, "A semiempirical model for interpreting microwave emission from semiarid land surfaces as seen from space," *IEEE Trans. Geosci. Rem. Sens., vol.* 28, pp. 384-393, 1990.

[16] M. Owe, A. A. van de Griend, and A. T. C. Chang, "Surface moisture and satellite microwave observations in semiarid southern Africa," *Water Resources Res.*, vol. 28, pp. 829-839, 1992.

[17] A. A. van de Griend and M. Owe, "Microwave vegetation optical depth and inverse model] ing of soil emissivity using Nimbus/SMMR satellite observations," *Meteorol. Amos. Phys.*, vol. 54, pp. 225-239, 1994.

[18] S. J. Sippel, S. K. Hamilton, J. M. Melack, and B. J. Choudhury, "Determination of inundation area in the Amazon river floodplain using the SMMR 37 GHz polarization difference," *Rem. Sens. Environ., vol.* 48, pp. 70-76, 1994.

[19] B. J. Choudhury, C. J. Tucker, R. E. Golus, and W. W. Newcomb, "Monitoring vegetation using Nimbus-7 scanning multichannel microwave radiometer's data," *Int. J. Rem. Sens.*, vol. 8, pp. 533-538, 1987.

[20] J.-C. Calvet, J.-P. Wigneron, E. Mougin, Y. H. Kerr, and J. S. Brito, "Plant water content and temperature of the Amazon forest from satellite microwave radiometry," *IEEE Trans. Geosci. Rem. Sens.*, vol. *32*, pp. 397-408, 1994.

[2 I] M. J. McFarland, R. L. Miller, and C. M. U. Neale, "Land surface temperature derived from the SSM/I passive microwave brightness temperatures," *IEEE Trans. Geosci. Rem. Sens., vol.* 28, pp. 839-845, 1990.

[22] E. G. Njoku, "Surface temperature estimation over land using satellite microwave radiometry," In: *Passive Microwave Remote Sensing of Land-Atmosphere Interactions (B. J. Choudhury, Y. H. Kerr, E. G. Njoku, and P. Pampaloni, Ms.),* VSP, Utrecht, The Netherlands, pp. 509-530, 1995.

[23] B. J. Choudhury, E. R. Major, E. A. Smith, and F. Becker, "Atmospheric effects on SMMR and SSM/I 37 GHz polarization difference over the Sahel," *Int. J. Rem. Sews.*, vol. 13, pp. 3443-3463, 1992.

[24] Y. *H.* Kerr and E. G. Njoku, "On the use of passive microwaves at 37 GHz in remote sensing of vegetation," *Int. J. Rem. Sens., vol.* 14, pp. 1931-1943, 1993.

[25] R. R. Ferraro, N. C. Grody, and J. A. Kogut, "Classification of geophysical parameters using passive microwave satellite measurements," *IEEE Trans. Geosci. Rem. Sens.*, vol. *24,* pp. 1008-1013, *1986.*

[26] C. M. U. Neale, M. J. McFarland, and K. Chang, "Land-surface-type classification using microwave brightness temperatures from the Special Sensor Microwave/Imager," *IEEE Trans. Geosci. Rem. Sens., vol. 28,* pp. 829-838, 1990.

[27] E. G. Njoku, S. J. Hook, and A. Chehbouni, "Effects of surface heterogeneity on thermal remote sensing of land parameters," In: *Scaling Up In Hydrology Using Remote Sensing (J. Stewart, E. Engman, R. Feddes, and Y. Kerr, Eds.),* Wiley, New York, pp. 19-37, 1995.

[28] D. Entekhabi, H. Nakamura, and E. G. Njoku, "Solving the inverse problem for soil moisture and temperature profiles by sequential assimilation of multifrequency remotely sensed observations," *IEEE Trans. Geosci. Rem. Sens.,* vol. *32,* pp. 438-448, 1994.

[29] D. LoSeen, A. Chehbouni, E. Njoku, and S. Saatchi, "A modeling study on the use of passive microwave data for the monitoring of sparsely vegetated land surfaces," *Proc. IEEE Geoscience and Remote Sensing Symposium (IGARSS'95),* Florence, Italy, 1995.

[30] T. Mo, B. J. Choudhury, T. J. Schmugge, J. R. Wang, and T. J. Jackson, "A model for microwave emission from vegetation covered fields," *J. Geophys. Res.,* vol. 87, pp. 11229-11237, 1982.

[31] T. J. Jackson and D. E. LeVine, "Mapping surface soil moisture using an aircraft-based passive microwave instrument: algorithm and example," *J. Hydrology,* vol. 184, pp. 85-99, 1996.

[32] L. Zurk, D. T. Davis, E. G. Njoku, L. Tsang, and J. N. Hwang, "Inversion of parameters for semiarid regions by a neural network," *Proc. IEEE Geoscience and Remote Sensing Symposium (IGARSS'92), Houston, TX,* pp. 1075-1077, 1992.

[33] E. G. Njoku, A. Chehbouni, F. Cabot, B. Rague, K. Fleming, and Y. H. Kerr, "An approach to estimating surface parameters and fluxes using modeling and multispectral remote sensing," *Proc. IEEE Geoscience and Remote Sensing Symposium (IGARSS'94), Pasadena, CA,* 1994.

[34] D. T. Davis, Z. Chen, J.-N. Hwang, L. Tsang, and E. G. Njoku, "Solving inverse problems by Bayesian iterative inversion of a forward model with applications to parameter mapping using SMMR remote sensing data," *IEEE Trans. Geosci. Rem. Sens.,* vol. 33, pp. 1182-1193, 1995.

[35] W. H. Press, W. H., B. P. Flannery, S. A. Teukolsky, and W. T. Vetterling, "*Numerical Recipes,* " Cambridge University Press, New York, (Ch. 14), 1989.

[36] NSIDC, "NSIDC DAAC Data Guide," *http://www-nsidc.colorado.edu/NASA/GUIDE/,* National Snow and Ice Data Center, Boulder, CO.

[37] J. R. Wang and B. J. Choudhury, "Remote sensing of soil moisture content over bare fields at 1.4 GHz frequency," *J. Geophys. Res., vol. 86,* pp. 5277-5282, 1981.

[38] J. R. Wang, P. E. O'Neill, T. J. Jackson, and E. T. Engman, "Multifrequency measurements of the effects of soil moisture, soil texture, and surface roughness," *IEEE Trans. Geosci. Rem. Sens., vol.21,* pp. 44-51, 1983.

[39] Y. H. Kerr and J. P. Wigneron, "Vegetation models and observations - A review," *In: Passive Microwave Remote Sensing of Land-Atmosphere Interactions (B. Choudhury, Y. Kerr, E. Njoku, and P. Pampaloni, Eds.), pp.3* 17-344, VSP, Utrecht, The Netherlands, 1995.

[40] E. Kalnay and 21 others, "The NCEP/NCAR 40-year reanalysis project," *Bull. Amer. Meteorol. Sot.,* vol. *77,* pp. 437-471, 1996.

[41] P. J. Sellers, and 14 others, "The ISLSCP Initiative I global datasets: Surface boundary conditions and atmospheric forcings for land-atmosphere studies," *Bull. Amer. Meteorol. Sot.,* vol. 77, pp. 1987-2005, 1996.

[42] J. R. Wang and T. J. Schmugge, "An empirical model for the complex dielectric permittivity of soil as a function of water content," *IEEE Trans. Geosci. Rem. Sens., vol. 18,* pp. *288-295, 1980.*

[43] M. C. Dobson, F. T. Ulaby, M. T. Hallikainen, and M. A. El-Rayes, "Microwave dielectric behaviour of wet soil -- Part 11: Dielectric mixing models," *IEEE Trans. Geosci. Rem. Sens.,* vol. 23, pp. 35-46, 1985.

[44] M. F. Wilson and A. Henderson-Sellers, "A global archive of land cover and soil data for use in general circulation climate models," *J. Climatol., vol.* 5, pp. 119-143, 1985.

[45] E. G. Njoku and J. A. Kong, "Theory for passive microwave remote sensing of near-surface soil moisture," *J. Geophys. Res., vol.* 82, pp. 3108-3118, 1977.

[46] T. T. Wilheit, "Radiative transfer in a plane stratified dielectric," *IEEE Trans. Geosci. Rem. Sens.*, vol. 16, pp. 138-143,1978.

[47] L. Tsang, J. A. Kong, and R. T. Shin, *"Theory of Microwave Remote Sensing, "* J. Wiley and Sons, New York, 1985.

[48] T. J. Jackson, "Measuring surface soil moisture **using** passive microwave remote sensing," *Hydrological Processes,* vol. 7, pp. 139-152, 1993.

[49] M. A. Karam, A. K. Fung, R. H. Lang, and N. S. Chauhan, "A microwave scattering model for layered vegetation," *IEEE Trans. Geosci. Rem. Sens.*, vol. 30, pp. 767-784, 1992..

[50] T. J. Jackson and T. J. Schmugge, "Vegetation effects on the microwave emission from soils," *Rem. Sens. Environ.,* vol. 36, pp. 203-212, 1991.

[51] U. Wegmuller, C. Matzler, and E. G. Njoku, "Canopy opacity models," *In: Passive Microwave Remote Sensing of Land-Atmosphere Interactions (B. Choudhury, Y. Kerr, E. Njoku, and P. Pampaloni, Eds.),* pp.375-387, VSP, Utrecht, The Netherlands, 1995.

[52] D. M. LeVine and M. A. Karam, "Dependence of attenuation in a vegetation canopy on frequency and plant water content," IEEE Trans. Geosci. Rem. Sens., vol. 34, pp. 1090-1096, 1996.

[53] W. B. Rossow and R. A. Schiffer, "ISCCP cloud data products," *Bull. Amer. Meteorol. Sot.,* vol. *72, pp. 2-20,* 1991.

Table 1: Comparative operating characteristics of SMMR, SSM/I, and AMSR

Parameter	SMMR (Nimbus-7)	SSM/I (DMSP)	AMSR-E (EOS PM-1)
Frequencies (GHz)	6.6, 10.7, 18,21,37	19.3,22 .3,37,85.5	6.9, 10.7, 18.7,23.8, 36.5,89
Altitude (km)	955	860	705
Antenna size (m)	0.79	0.6	1.6
Incidence angle (deg)	50.3	53.1	55
Footprint size (km) at 6.6 GHz at 37 GHz	 95 x 148 18x27	 N/A 28 x 37	 43 x 75 8 x 14
Swath width (km)	780 “	1400	**1445**
Launch date	(1978—No longer operating)	(1 987—Series in orbit)	**2000**

Table 2: Parameters of the Microwave Model

Parameter	Description
(a) Media & Sensor Parameters	
Atmosphere:	
τ_o	Oxygen nadir opacity
a_v, a_l	Water vapor and liquid opacity coefficients
δT_a	Lapse-rate temperature differential (K)
Vegetation:	
ω_p	Single scattering albedo
b	Opacity coefficient
Soil:	
h, Q	Roughness coefficients
ρ_b	Bulk density (g cm^{-3})
s, c	Sand and clay mass fractions
Sensor:	
θ	Viewing angle (deg)
v	Frequency (GHz)
p	Polarization
(b) Media Variables	
Atmosphere:	
q_v	Precipitable water (cm)
q_l	Cloud liquid water path (mm)
T_{as}	Surface air temperature (K)
Land Surface:	
m_e	Surface soil moisture (g cm^{-3})
w_e	Vegetation water content (kg m^{-2})
T_e	Surface temperature (K)

Table *3:* Normalized sensitivities at 6.6 GHz H and V polarizations, θ = 50.3°, for given parameter ranges X_j, and baseline values x_{oj}.

Parameter	Range (X_j)	Baseline (x_{oj})	Sensitivity, H S'_{ij}(K)	Sensitivity, V S_{ij}(K)
(a) *Vegetation baseline = O kg m^{-2} (bare soil):*				
Soil moisture (g cm^{-3})	*0.32*	**0.15**	*95.5*	*60.1*
Surface temperature (“C)	**40**	**20**	*25.1*	*35.7*
Vegetation water (kg m^{-2})	**1.5**	**0**	*211.3*	*28.1*
Atmos. Water Vapor (mm)	**5**	*2.5*	*1.3*	*0.18*
(a) Vegetation baseline = 1.5 kg m^{-2}:				
Soil moisture (g cm^{-3})	*0.32*	**0.15**	*8.5*	*5.3*
Surface temperature (“C)	**40**	**20**	*22.0*	*20.6*
Vegetation water (kg m^{-2})	**1.5**	**1,5**	*10.9*	1.2
Atmos. Water Vapor (mm)	**5**	**2.5**	*0.12*	*0.02*

Table 4: Means and standard deviations of simulated retrieval errors for m_e, w_e, T_e, and q_v, for two cases of sensor noise: (a) $AT = 0.3$ K; (b) $AT = 0.5$ K. Values are averages over 10 sets of $n_r = 200$ sensor noise realizations.

Variable	Mean Error	Standard Deviation of Error
(a) $\Delta T = 0.3$ K		
m_e (g cm^{-3})	-2.9 $\times 10^{-4}$	0.018
w_e (kg m^{-2})	4.8 $\times 10^{-4}$	0.029
T_e (C)	-0.034	0.80
q_v (cm)	-0.039	1.46
(b) $\Delta T = 0.5$ K		
m_e (g cm^{-3})	3.8 $\times 10^{-4}$	0.028
w_e (kg m^{-2})	-1.3X 10^{-3}	0.051
T_e (C)	-0.028	1.24
q_v (cm)	0.11	1.92

Table 5: Model parameters, h, Q, and ω_p (horizontal and vertical polarizations) derived over the desert and forest calibration sites.

Frequency (GHz)	h	Q	ω_h	ω_v
6.6	0.11	0.09	0.11	0.08
10.7	0.19	0.11	0.10	0.08
18	0.14	0.12	0.11	0.09

Figure 1: Brightness temperatures computed at the SMMR frequencies (6.6, 10.7, and 18 GHz; V and H polarizations) and viewing angle (θ = 50.30), as functions of: (a) soil moisture, m_e; (b) vegetation water content, w_e; (c) surface temperature, T_e; (d) precipitable water, q_v; and (e) cloud liquid water path, q_l.

Figure 2: Scatterplots of simulated 'retrieved' versus 'true' parameters for one set of realizations n_r = 200, and sensor noise $A\,T = 0.3$ K. Retrieved parameters are asterisked. (a) Soil moisture; (b) Vegetation water content; (c) Surface temperature; (cl) Precipitable water.

Figure 3: Histograms of the simulated retrieval errors ('retrieved' minus 'true') for the same realizations and sensor noise as in Figure 2. (a) Soil moisture; (b) Vegetation water content; (c) Surface temperature; (d) Precipitable water. The horizontal axes of the histograms are normalized to the parameter ranges: $\Delta m_e = \pm 0.15$ g cm^{-3}; $\Delta w_e = \pm 0.75$ kg m^{-2}; $\Delta T_e = \pm 20$ C; $\Delta q_v = \pm 2.5$ cm.

Figure 4: Simulated retrieval errors $\varepsilon_m, \varepsilon_w, \varepsilon_T$, and ε_q, for soil moisture, vegetation water content, surface temperature, and precipitable water, respectively, as functions of the 'true' values m_e, w_e, T_e, and q_v. Solid lines are the mean errors, and dashed lines are the error standard deviations. Instrument noise of $AT = 0.3$ K is assumed. (See text for discussion.)

Figure 5: Rectangular area is shown over which retrievals using SMMR data and NCEP model output data were averaged for the comparisons shown in Figure 6. Also shown are the locations: A - Desert, and B - Forest, that were used as calibration sites for the SMMR retrieval algorithm.

Figure 6: Comparisons between SMMR retrievals and NCEP model output data, averaged over the region shown in Figure 5, for the years 1982 through 1985. (a) SMMR retrievals of soil moisture, m_e, vegetation water content, w_e, and surface temperature, T_e, and NCEP model-derived precipitation rate, P. (b) SMMR retrievals of m_e and T_e compared against NCEP-derived surface soil moisture, *Soilw*, and surface temperature, *Tsfc*. The units have been scaled as indicated for convenience.

Figure 7: ScatterPlots of SMMR-derived versus NCEP model output variables: (a) m_e (SMMR) vs. *Soilw* (NCEP); (b) T_e (SMMR) vs. *Tsfc* (NCEP). The best fit regression lines are shown dotted.

Fig 1

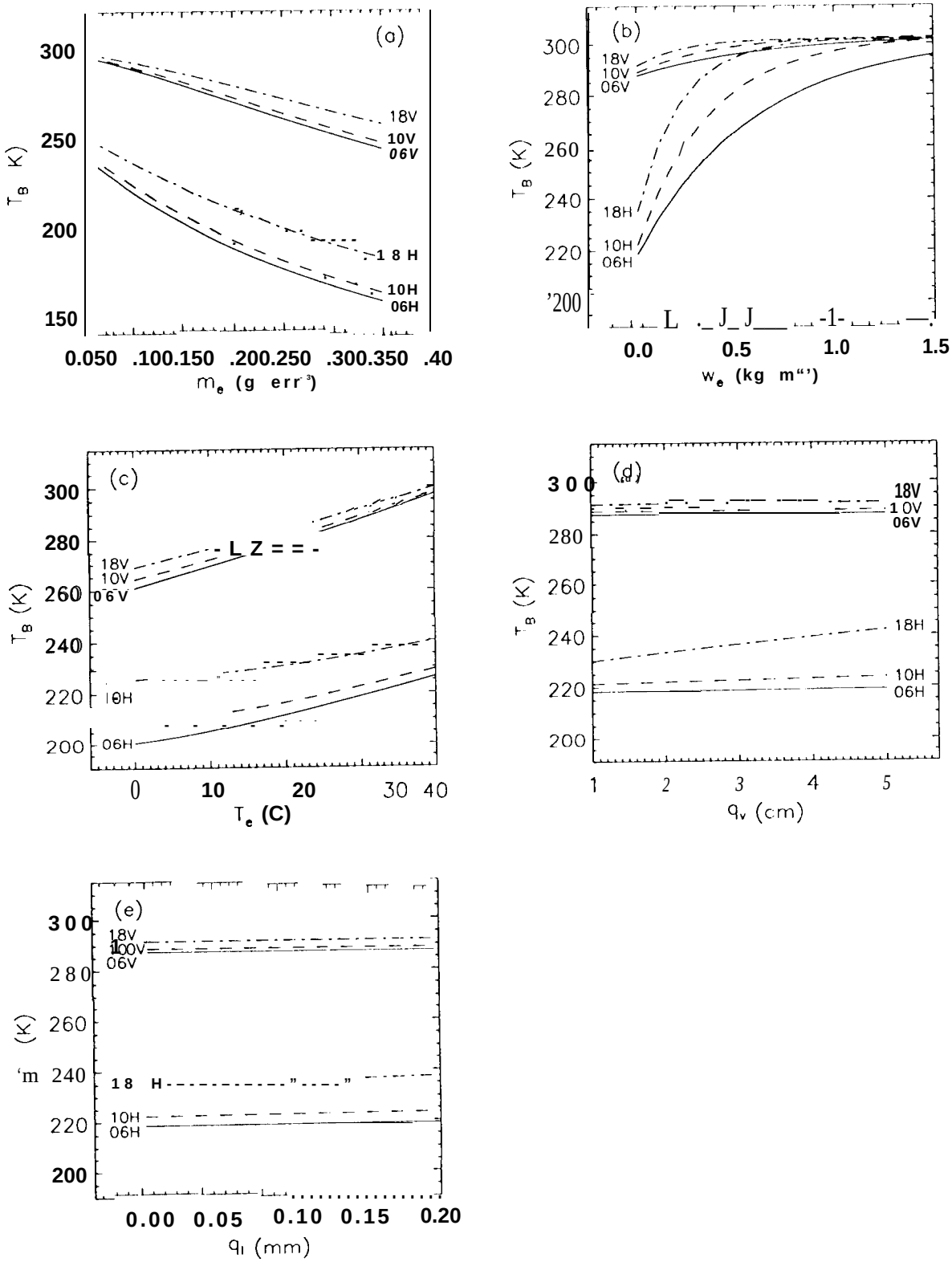
(a)
300
250
200
150
T_B K)
18V
10V
06V
18H
10H
06H
0.050 .100.150 .200.250 .300.350 .40
m_e (g err^3)
(b)
300
280
260
240
220
'200
T_B (K)
18V
10V
06V
18H
10H
06H
0.0 0.5 1.0 1.5
w_e (kg m"')
(c)
300
280
260
240
220
200
T_B (K)
18V
10V
06V
10H
06H
0 10 20 30 40
T_e (C)
(d)
300
280
260
240
220
200
T_B (K)
18V
10V
06V
18H
10H
06H
1 2 3 4 5
q_v (cm)
(e)
300
280
260
240
220
200
(K)
'm
18V
10V
06V
18H
10H
06H
0.00 0.05 0.10 0.15 0.20
q_l (mm)

Fig 2

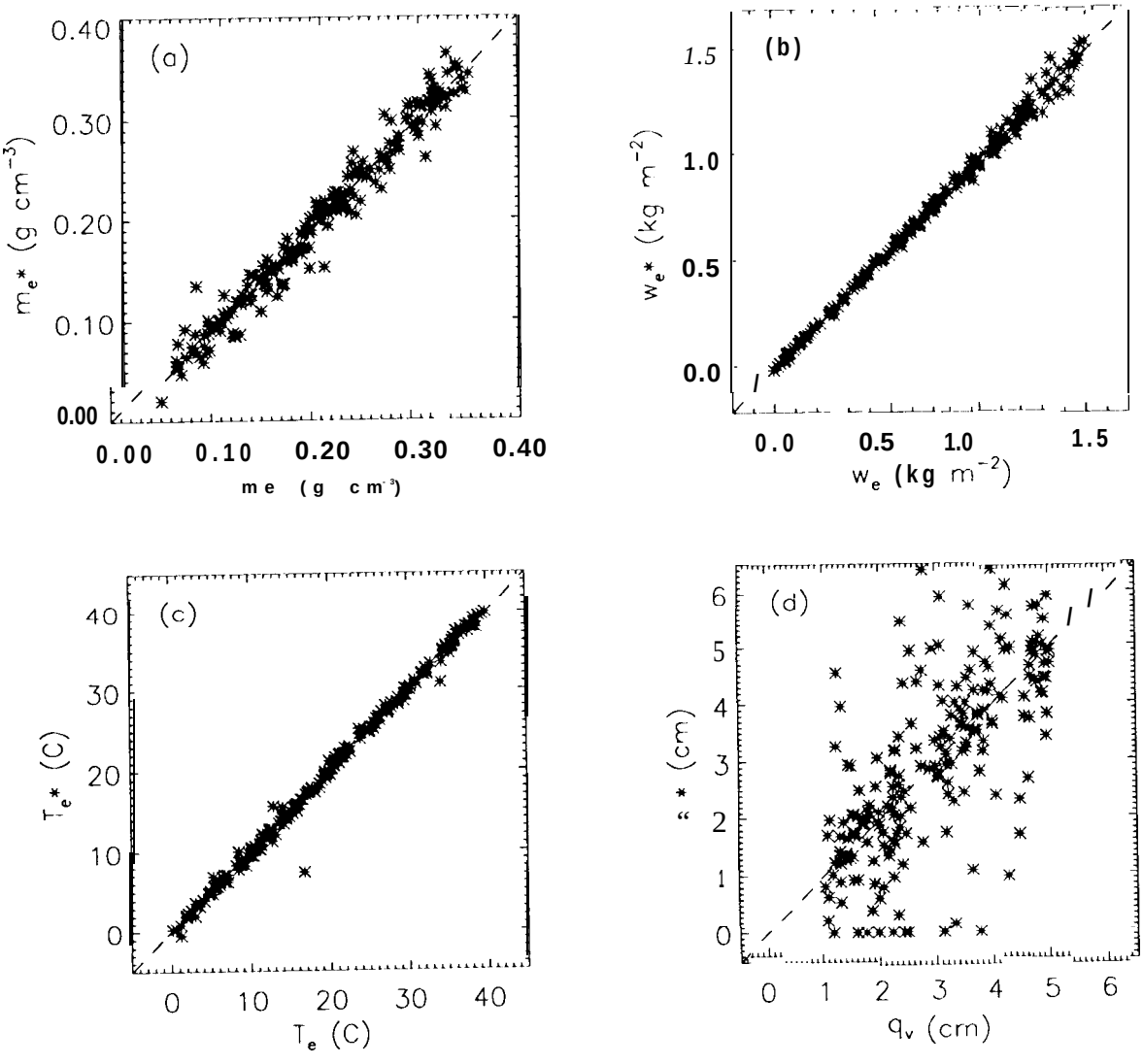
(a)
0.40
0.30
0.20
0.10
0.00
m_e^* (g cm^{-3})
0.00 0.10 0.20 0.30 0.40
me (g cm^{-3})
(b)
1.5
1.0
0.5
0.0
w_e^* (kg m^{-2})
0.0 0.5 1.0 1.5
w_e (kg m^{-2})
(c)
40
30
20
10
0
T_e^* (C)
0 10 20 30 40
T_e (C)
(d)
6
5
4
3
2
1
0
q_v^* (cm)
0 1 2 3 4 5 6
q_v (cm)

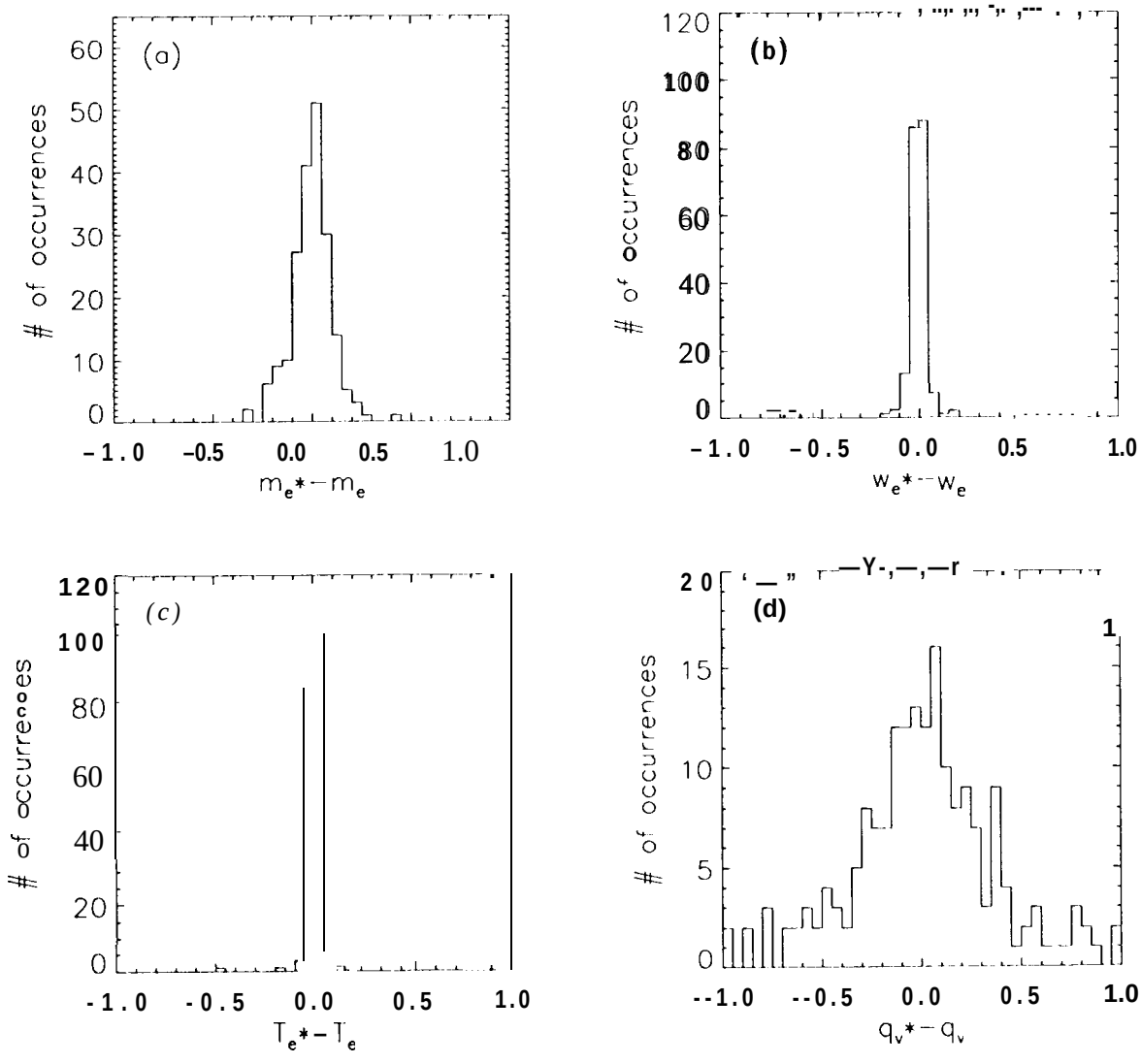
(a)
# of occurrences
60
50
40
30
20
10
0
-1.0
-0.5
0.0
0.5
1.0
$m_e^* - m_e$
(b)
# of occurrences
120
100
80
60
40
20
0
-1.0
-0.5
0.0
0.5
1.0
$w_e^* - w_e$
(c)
# of occurrences
120
100
80
60
40
20
0
-1.0
-0.5
0.0
0.5
1.0
$T_e^* - T_e$
(d)
# of occurrences
20
15
10
5
0
--1.0
--0.5
0.0
0.5
1.0
$q_v^* - q_v$

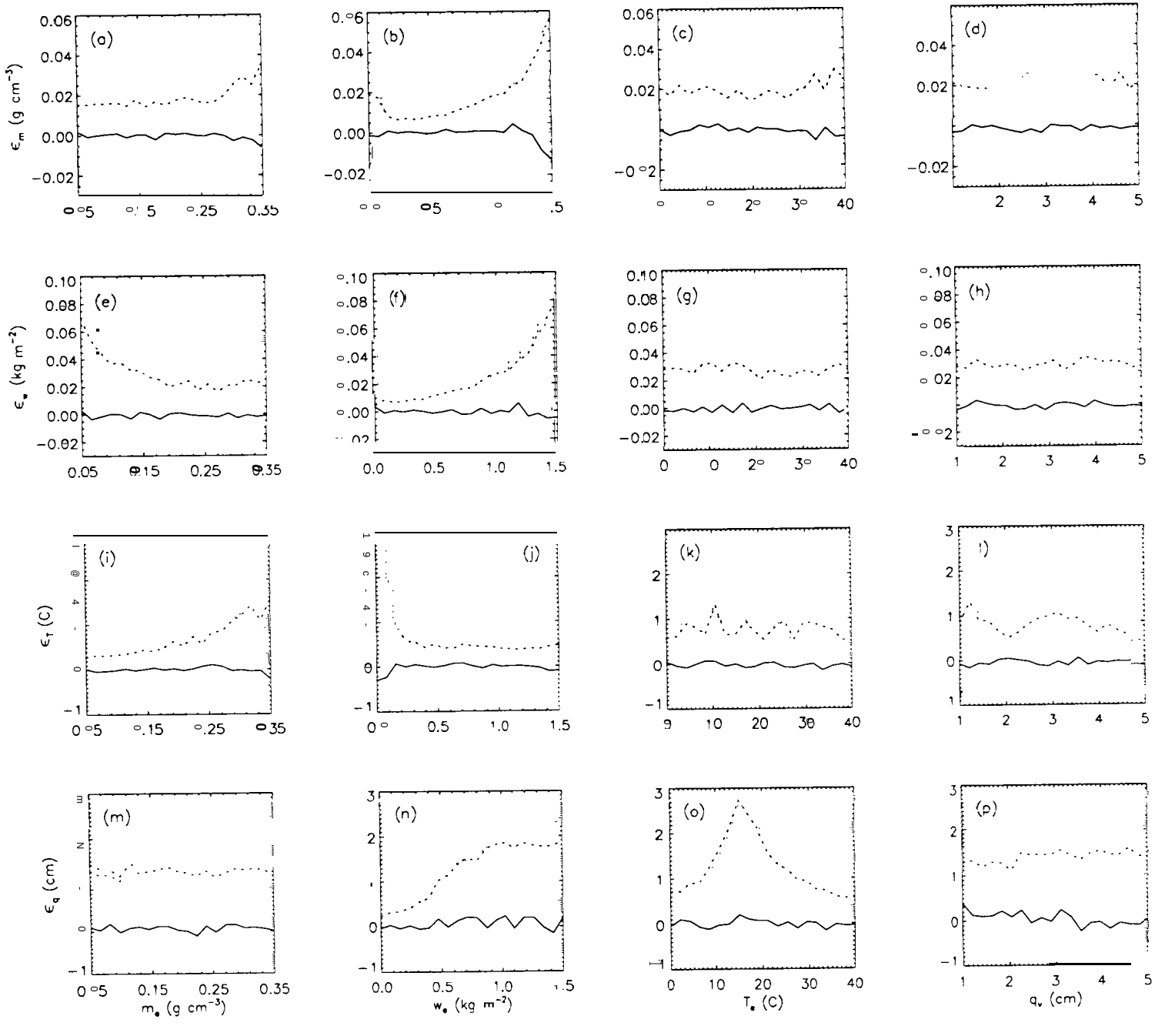

Fig 4

Figure 4

Figure 5

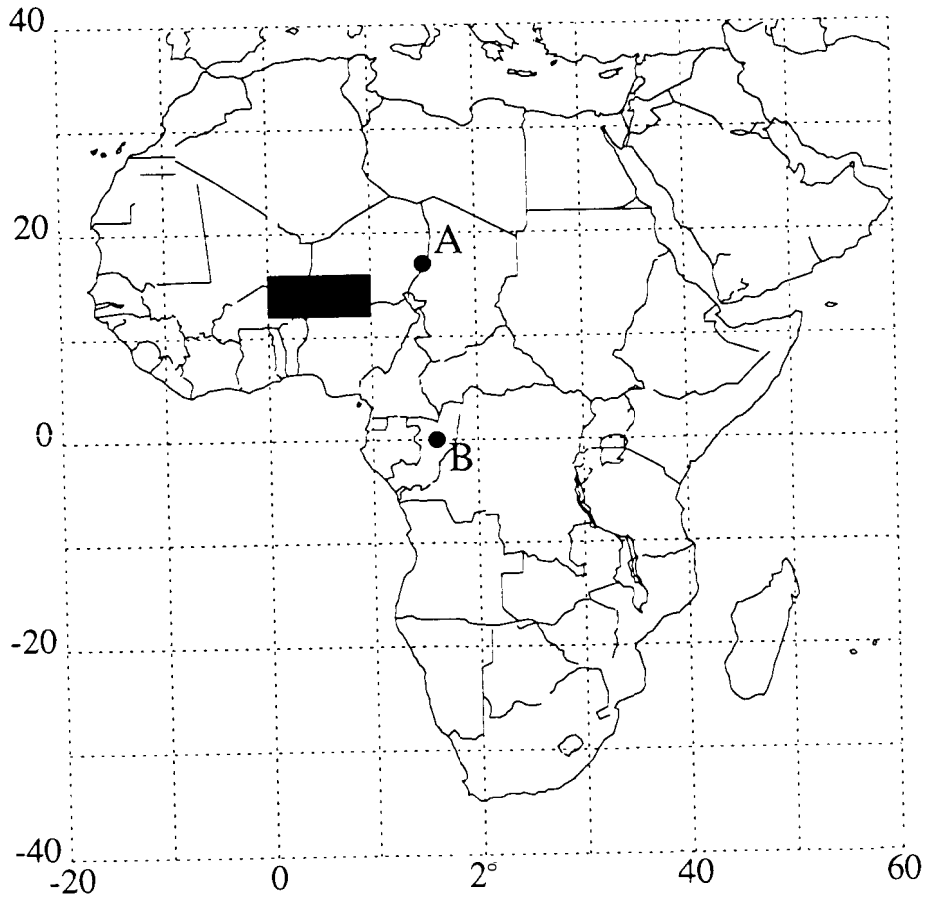

Figure 6(a)

Fig 6(a)

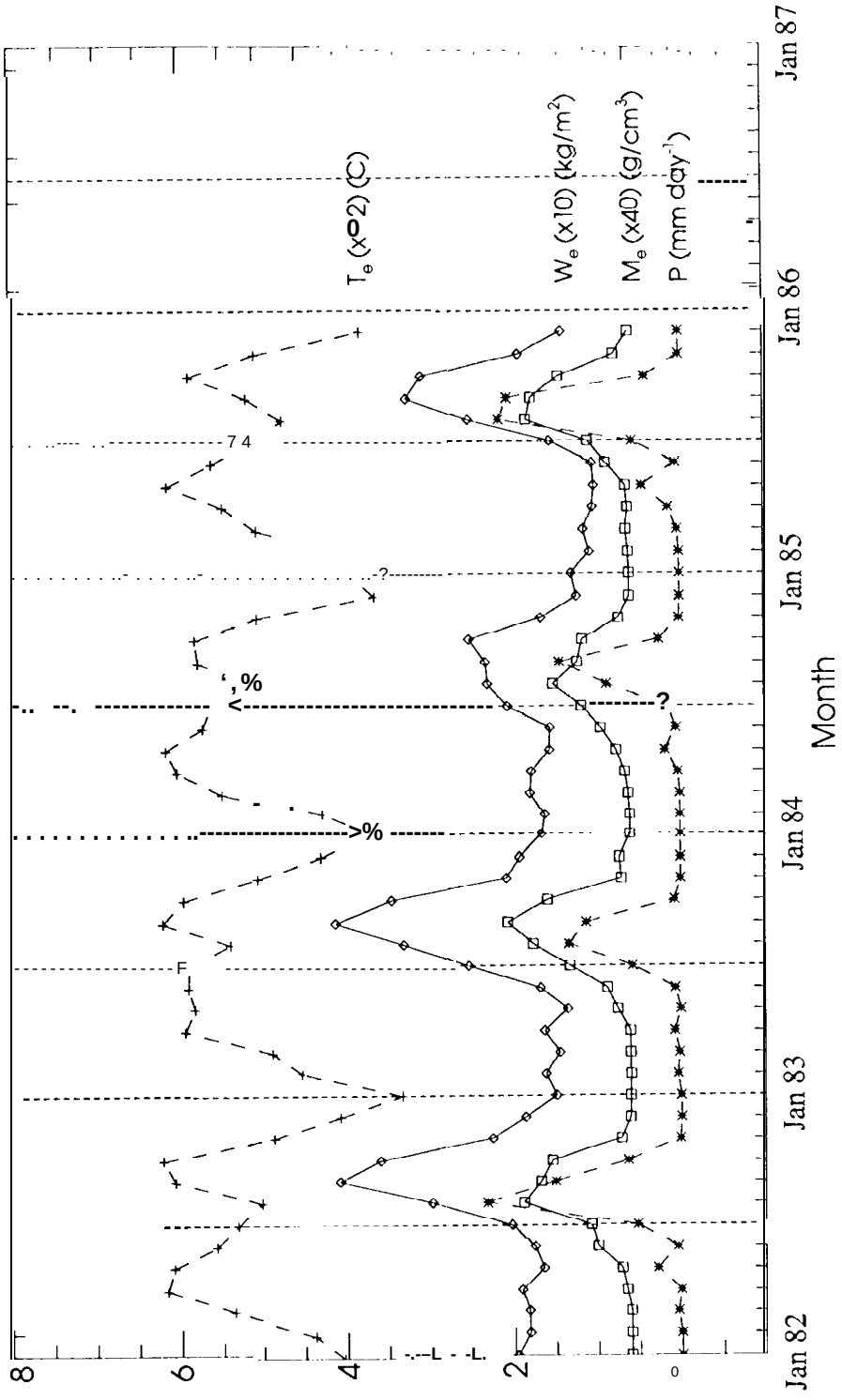

Figure 6(k

Fig. 6(

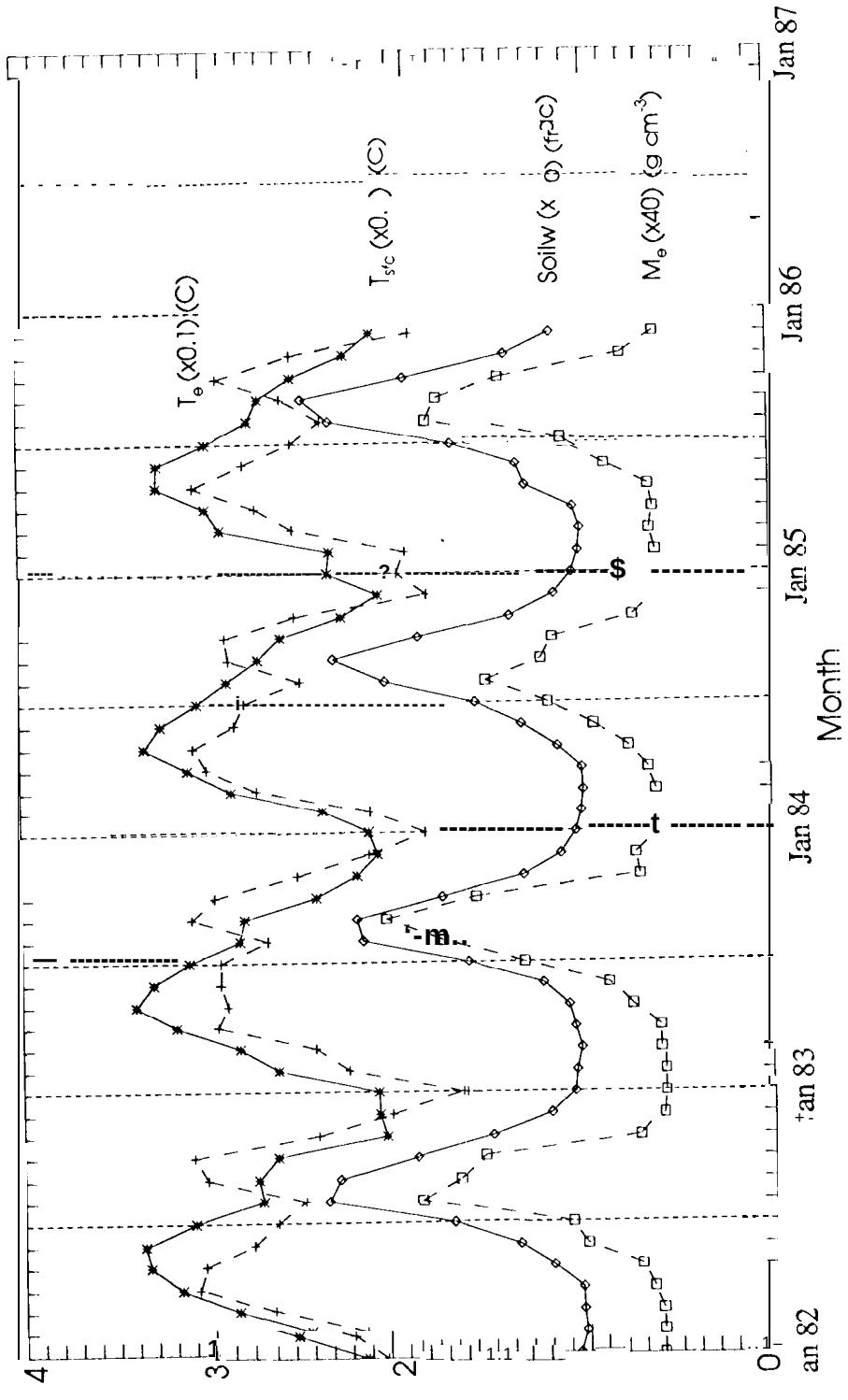

Fig 7

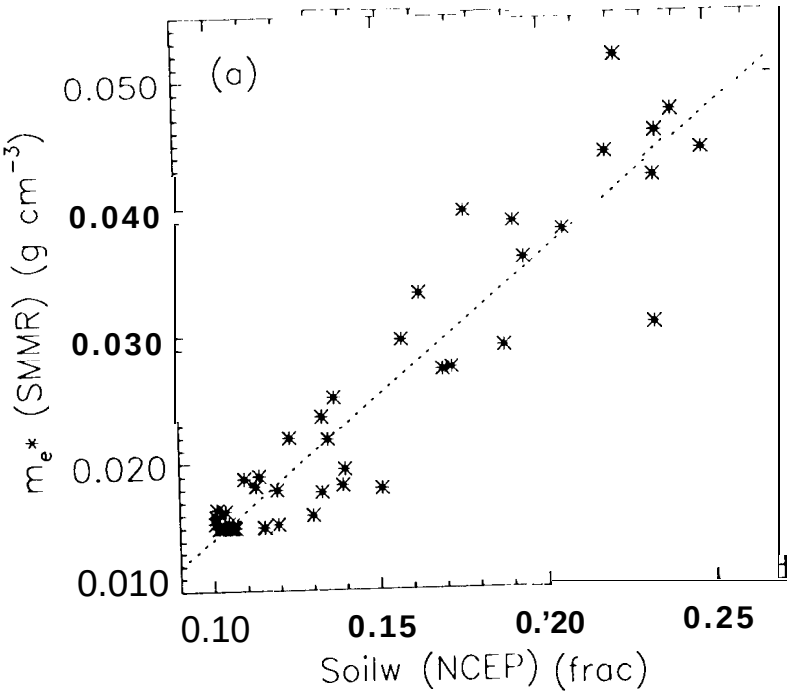
(a)
0.050
0.040
0.030
0.020
0.010
m_e^* (SMMR) (g cm^{-3})
0.10
0.15
0.'20
0.25
Soilw (NCEP) (frac)

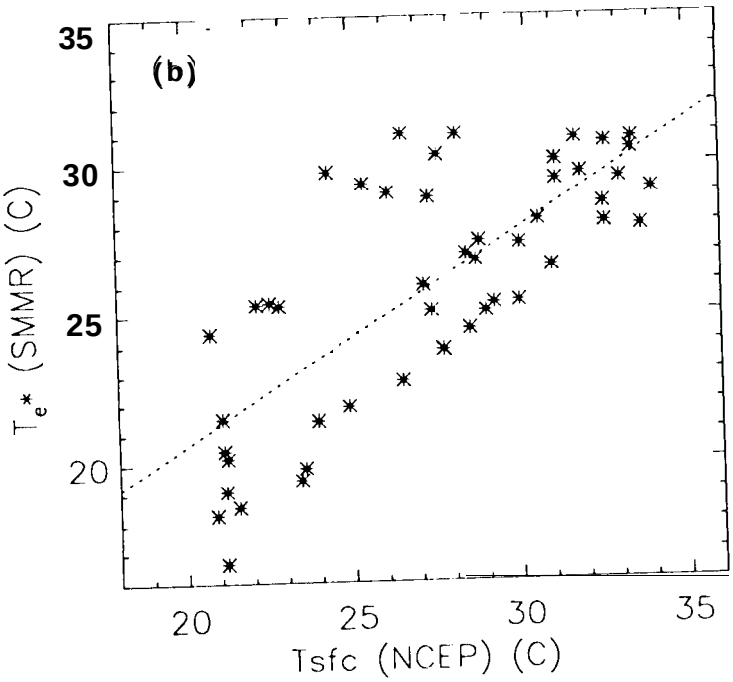
(b)
35
30
25
20
T_e^* (SMMR) (C)
20
25
30
35
Tsfc (NCEP) (C)